GMR
The Original

FORMULATION DEVELOPMENT OF CELASTROL POLYMERIC NANOPARTICLES AS A NANO-THERAPEUTIC APPROACH FOR RHEUMATOID ARTHRITIS

[1]Narendra C, [2]Sujatha, [3]*Deepali Maruti Jagdale, [4]Gunjan Rani, [5]Senthil Rajan Dharmalingam, [6]Arghya Paria, [7]Rita Yadav, [8]G. Sai Sruti

[1, 2]Department of Pharmaceutics, Visveswarapura Institute of Pharmaceutical Sciences, BSK II stage, Bangalore. 560070
[3]Associate Professor, Department of Pharmaceutical Chemistry, Bharati Vidyapeeth's College of Pharmacy, Sector 8, CBD Belapur, Navi Mumbai, Maharashtra, India. 400614
[4]Professor, School of Pharmacy, Mangalayatan University, Aligarh, Uttar Pradesh, India.
[5]Department of Pharmaceutics, Swamy Vivekananda College of Pharmacy, "Affiliated to TN Dr. MGR Medical University, Chennai" Tiruchengodu, Namakkal - 637 205, India.
[6]Assistant Professor "Haldia Institute of Pharmacy, Haldia, East Midnapore, West Bengal. 721657"
[7]Assistant Professor, School of Pharmaceutical Sciences, Faculty of Pharmacy, IFTM University Lodhipur, Rajput Moradabad, Uttar Pradesh. 244102
[8]Assistant Professor, Royal College of Pharmacy and Health Sciences, Andhapasara Road, Berhampur, Ganjam, Odisha,.760002
*Corresponding Author: Deepali Maruti Jagdale, Email: deepali.jagdale@bvcop.in

ABSTRACT

Celastrol is a bioactive pentacyclic triterpenoid with potent anti-inflammatory activity, but its pharmaceutical development is restricted by extremely poor aqueous solubility, limited bioavailability, rapid systemic elimination, and concentration-dependent toxicity. The present study aimed to develop and optimize Celastrol-loaded PEGylated PLGA nanoparticles for improved in vitro anti-inflammatory performance relevant to rheumatoid arthritis. Nanoparticles were prepared by nanoprecipitation using PLGA and mPEG-PLGA at a fixed 80:20 w/w ratio and optimized through a three-factor, three-level Box–Behnken Design. Total polymer concentration, Poloxamer 188 concentration, and Celastrol-to-total-polymer ratio were evaluated against particle size, entrapment efficiency, and drug release at 24 h. The optimized formulation exhibited a mean particle size of 150.6 ± 3.4 nm, PDI of 0.186 ± 0.012, zeta potential of −24.8 ± 1.7 mV, entrapment efficiency of 87.1 ± 1.5%, and sustained drug release of 93.1 ± 1.3% over 48 h. FTIR, DSC, PXRD, and TEM analyses confirmed drug–polymer compatibility, reduced Celastrol crystallinity, and spherical nanoparticle morphology. In LPS-stimulated RAW 264.7 macrophages, Celastrol nanoparticles showed improved cellular tolerability and significantly reduced intracellular reactive oxygen species, nitric oxide production, and secretion of TNF-α, IL-6, and IL-1β compared with free Celastrol. The formulation remained physically stable during three months of storage. These findings demonstrate that PEGylated PLGA nanoparticles can improve the pharmaceutical performance and in vitro anti-inflammatory activity of Celastrol and warrant further investigation in rheumatoid arthritis models.

KEYWORDS: Celastrol; PLGA nanoparticles; PEGylation; rheumatoid arthritis; macrophages; anti-inflammatory activity

1. INTRODUCTION

Rheumatoid arthritis (RA) is a chronic, systemic autoimmune disorder characterized by persistent synovial inflammation, progressive cartilage destruction, and bone erosion, ultimately leading to joint deformity and disability. The disease affects approximately 0.5–1% of the global population and is associated with substantial socioeconomic burden and reduced quality of life. Although the precise etiology of RA remains incompletely understood, the pathogenesis involves a complex interaction between genetic susceptibility, environmental factors, and dysregulated immune responses. Activated macrophages, T lymphocytes, fibroblast-like synoviocytes, and various inflammatory mediators contribute to the perpetuation of chronic inflammation and irreversible joint damage (C. Li *et al.*, 2022; Lin *et al.*, 2022; Mino *et al.*, 2021; Mori *et al.*, 2021; Ozdemir *et al.*, 2009; Quan *et al.*, 2021).

Macrophages play a central role in RA progression through excessive production of pro-inflammatory cytokines and reactive oxygen species. Elevated levels of tumor necrosis factor-alpha (TNF-α), interleukin-6 (IL-6), and interleukin-1β (IL-1β) are commonly observed in rheumatoid joints and are strongly associated with synovial hyperplasia, cartilage degradation, angiogenesis, and osteoclast activation. Moreover, increased oxidative stress and nitric oxide production further amplify inflammatory signaling pathways, contributing to tissue injury and disease progression. Consequently, suppression of macrophage-mediated inflammatory responses has emerged as an important therapeutic strategy in rheumatoid arthritis management (Elkomy *et al.*, 2022; Guo *et al.*, 2022; Gupta *et al.*, 2022; Hu *et al.*, 2022; Mori *et al.*, 2021; Quan *et al.*, 2021). Current treatment approaches for RA primarily include nonsteroidal anti-inflammatory drugs, corticosteroids, conventional disease-modifying antirheumatic drugs (DMARDs), and biological agents targeting specific inflammatory mediators. Despite significant advances in treatment, these therapies are frequently associated with limitations including poor patient response, systemic adverse

effects, high treatment costs, increased risk of infections, and the requirement for long-term administration. Therefore, the development of safer and more effective therapeutic approaches capable of modulating multiple inflammatory pathways remains an important research objective (Du *et al.*, 2021; Higashiguchi *et al.*, 2021; Quan *et al.*, 2021; Schattner, 2023; Shao *et al.*, 2023; Singh *et al.*, 2023).

Celastrol, a quinone methide pentacyclic triterpenoid isolated mainly from *Tripterygium wilfordii* Hook F., has attracted considerable attention owing to its potent anti-inflammatory, antioxidant, immunomodulatory, and anticancer activities. Numerous studies have demonstrated that Celastrol suppresses activation of nuclear factor-kappa B (NF-κB), inhibits production of pro-inflammatory cytokines, reduces oxidative stress, and modulates multiple signaling pathways implicated in autoimmune disorders. In experimental models of rheumatoid arthritis, Celastrol has shown significant therapeutic potential by attenuating inflammatory responses and reducing joint destruction (Cui *et al.*, 2024; Qiu *et al.*, 2021; Tan *et al.*, 2023; Xian *et al.*, 2021; Zhang *et al.*, 2022). However, the clinical translation of Celastrol remains challenging because of several unfavourable pharmaceutical characteristics. The compound exhibits extremely poor aqueous solubility limited oral bioavailability, rapid metabolism, and concentration-dependent systemic toxicity. Furthermore, its hydrophobic nature often results in poor dispersion in biological fluids and inconsistent therapeutic exposure. These limitations necessitate the development of an appropriate delivery system capable of improving its physicochemical properties while maintaining therapeutic activity (Y. Li *et al.*, 2025; Liu *et al.*, 2025; Mias *et al.*, 2023; Qi *et al.*, 2025).

Polymeric nanoparticles have emerged as promising drug-delivery systems for poorly soluble molecules because they can enhance apparent solubility, improve drug stability, prolong release, and increase cellular interaction. Among various polymeric carriers, poly(D,L-lactide-co-glycolide) (PLGA) has received considerable attention owing to its biodegradability, biocompatibility, and regulatory acceptance. Incorporation of polyethylene glycol (PEG) into PLGA systems further improves colloidal stability and provides steric stabilization, reducing nanoparticle aggregation and potentially improving biological performance (Chung *et al.*, 2010; da Silva *et al.*, 2013; Danhier *et al.*, 2009; Garinot *et al.*, 2007; Kumar *et al.*, 2013; Liang *et al.*, 2009; Lü *et al.*, 2009). Encapsulation of Celastrol within PEGylated PLGA nanoparticles may therefore overcome several limitations associated with the free drug by providing controlled release and improved cellular delivery. Moreover, macrophages readily internalize nanoparticles within the nanometer size range, making polymeric nanocarriers particularly attractive for modulation of inflammatory pathways involved in rheumatoid arthritis (Hoyos-Ceballos *et al.*, 2020; Kennedy *et al.*, 2018; Kumar *et al.*, 2013; Thakur *et al.*, 2016; Yang *et al.*, 2012).

Based on these considerations, the present study aimed to develop and optimize PEGylated PLGA nanoparticles of Celastrol using the nanoprecipitation technique and Box–Behnken experimental design. The prepared nanoparticles were characterized with respect to their physicochemical properties, drug-release behavior, and stability. Furthermore, their anti-inflammatory potential was evaluated in lipopolysaccharide-stimulated RAW 264.7 macrophages by assessing cellular viability, intracellular reactive oxygen species generation, nitric oxide production, and pro-inflammatory cytokine secretion. The study sought to establish a rational polymeric nanocarrier system capable of improving the pharmaceutical performance and in vitro anti-inflammatory activity of Celastrol for potential future application in rheumatoid arthritis therapy.

2. MATERIALS AND METHODS

2.1 Materials

Celastrol (purity ≥98%) was procured from MedChemExpress (USA). Poly(D,L-lactide-co-glycolide) (PLGA; 50:50, molecular weight 30,000–60,000 Da) and methoxy polyethylene glycol-poly(D,L-lactide-co-glycolide) (mPEG-PLGA) were purchased from Sigma-Aldrich (USA). Poloxamer 188 was obtained from BASF (Germany). Acetone, methanol, ethanol, dimethyl sulfoxide (DMSO), and acetonitrile of HPLC grade were procured from Merck (India). Dulbecco's Modified Eagle Medium (DMEM), fetal bovine serum (FBS), penicillin–streptomycin solution, trypsin, MTT reagent, lipopolysaccharide (LPS), dichlorofluorescein diacetate (DCF-DA), and Griess reagent were purchased from HiMedia Laboratories (India). ELISA kits for tumor necrosis factor-alpha (TNF-α), interleukin-6 (IL-6), and interleukin-1β (IL-1β) were procured from Elabscience Biotechnology Inc. (USA). Ultrapure water generated using a Milli-Q purification system was used throughout the study.

Table 1. List of chemicals used in the study

Chemical/Reagent	Grade	Supplier
Celastrol	≥98% purity	MedChemExpress, USA
PLGA (50:50)	Pharmaceutical grade	Sigma-Aldrich, USA
mPEG-PLGA	Pharmaceutical grade	Sigma-Aldrich, USA
Poloxamer 188	Pharmaceutical grade	BASF, Germany
Acetone	HPLC grade	Merck, India
Methanol	HPLC grade	Merck, India
Acetonitrile	HPLC grade	Merck, India
DMSO	Analytical grade	Merck, India
DMEM	Cell culture grade	HiMedia, India
FBS	Cell culture grade	HiMedia, India
MTT reagent	Cell culture grade	HiMedia, India

LPS	Cell culture grade	HiMedia, India
DCF-DA	Analytical grade	HiMedia, India
ELISA kits	Analytical grade	Elabscience, USA

Table 2. Major instruments employed in the study

Instrument	Manufacturer
UV–Visible spectrophotometer	Shimadzu, Japan
HPLC system	Waters, USA
Probe sonicator	Sonics Vibra Cell, USA
Dynamic light scattering analyzer	Malvern Zetasizer Nano ZS, UK
Differential scanning calorimeter	PerkinElmer, USA
FTIR spectrometer	Bruker Alpha, Germany
Powder X-ray diffractometer	Rigaku, Japan
Transmission electron microscope	JEOL, Japan
Microplate reader	BioTek, USA
CO_2 incubator	Thermo Fisher Scientific, USA

2.2 Preformulation Studies

2.2.1 Solubility Studies

The solubility of Celastrol was determined in distilled water, methanol, ethanol, acetone, DMSO, and phosphate buffer (pH 7.4). Excess Celastrol was added to 5 mL of each solvent and shaken continuously at 25 ± 1°C for 72 h using an orbital shaker. The suspensions were centrifuged at 10,000 rpm for 15 min and filtered through a 0.22 µm membrane filter. The drug concentration was quantified using HPLC analysis (Alves *et al.*, 2022; Ostróżka-Cieślik, 2025; Steele & Austin, 2016).

2.2.2 Fourier Transform Infrared Spectroscopy (FTIR)

FTIR analysis was performed to evaluate possible drug–excipient interactions. Spectra of pure Celastrol, PLGA, mPEG-PLGA, physical mixtures, and optimized nanoparticles were recorded using the potassium bromide pellet method over the spectral range of 4000–400 cm^{-1} (Alves *et al.*, 2022; Ostróżka-Cieślik, 2025; Steele & Austin, 2016).

2.2.3 Differential Scanning Calorimetry (DSC)

Thermal characteristics of the pure drug, polymers, physical mixture, and optimized formulation were analyzed using differential scanning calorimetry. Approximately 5 mg of sample was placed in sealed aluminium pans and heated from 30°C to 300°C at a rate of 10°C/min under nitrogen atmosphere (Alves *et al.*, 2022; Ostróżka-Cieślik, 2025; Steele & Austin, 2016).

2.2.4 Powder X-ray Diffraction (PXRD)

The crystalline characteristics of Celastrol before and after encapsulation were examined using powder X-ray diffraction. Samples were scanned between 5° and 50° (2θ) at a scanning rate of 2°/min (Alves *et al.*, 2022; Ostróżka-Cieślik, 2025; Steele & Austin, 2016).

2.3 Experimental Design

A three-factor, three-level Box–Behnken Design (BBD) was employed using Design-Expert® software to optimize Celastrol-loaded polymeric nanoparticles (Desai *et al.*, 2026; Kokatanur *et al.*, 2026; Rahali *et al.*, 2025; Rathore *et al.*, 2025).

Independent variables:

- A: PLGA concentration (%)
- B: Poloxamer 188 concentration (%)
- C: Drug-to-polymer ratio

Dependent variables:

- Y_1: Particle size (nm)
- Y_2: Entrapment efficiency (%)
- Y_3: Cumulative drug release at 24 h (%)

Seventeen experimental runs including five center points were generated.

Table 3. Experimental variables and levels

Factor	Symbol	Low (-1)	Medium (0)	High (+1)
PLGA concentration (%)	A	0.5	1.0	1.5
Poloxamer concentration (%)	B	0.2	0.6	1.0
Drug:Polymer ratio	C	1:5	1:10	1:15

2.4 Preparation of Celastrol-Loaded Polymeric Nanoparticles

Celastrol-loaded PEGylated PLGA nanoparticles were prepared by the nanoprecipitation technique. Briefly, accurately weighed quantities of Celastrol, PLGA, and mPEG-PLGA were dissolved in acetone to obtain the organic phase. The aqueous phase consisted of Poloxamer 188 dissolved in distilled water. The organic phase was added

dropwise into the aqueous phase under magnetic stirring at 1000 rpm. The resulting nanosuspension was subjected to probe sonication for 3 min in pulse mode to reduce particle size and improve homogeneity. Organic solvent removal was achieved by continuous stirring at room temperature for 4 h. The nanoparticles obtained were centrifuged at 18,000 rpm for 30 min at 4°C and washed twice with distilled water to remove unentrapped drug and excess surfactant. The final nanoparticle dispersion was lyophilized using mannitol (5% w/v) as cryoprotectant and stored at 4°C until further evaluation (Damiri *et al.*, 2026; Kataki; Kesharwani *et al.*, 2026; Kiani *et al.*, 2026; H. Li *et al.*, 2025; Mohamed *et al.*, 2025; Rajkumari *et al.*, 2024; Sathishbabu *et al.*, 2025; Zhao *et al.*, 2025).

2.5 Characterization of Polymeric Nanoparticles

2.5.1 Particle Size, Polydispersity Index and Zeta Potential

The mean particle size, polydispersity index (PDI), and zeta potential of the formulations were determined using dynamic light scattering. Samples were diluted appropriately with filtered distilled water before measurement. All analyses were performed in triplicate at 25°C (Damiri *et al.*, 2026; Kesharwani *et al.*, 2026; Kiani *et al.*, 2026; H. Li *et al.*, 2025; Mohamed *et al.*, 2025; Sathishbabu *et al.*, 2025; Zhao *et al.*, 2025).

2.5.2 Determination of Entrapment Efficiency

Entrapment efficiency was determined by the indirect method. Nanoparticle dispersions were centrifuged at 18,000 rpm for 30 min and the amount of free drug present in the supernatant was quantified using HPLC. Entrapment efficiency was calculated according to the following equation (Damiri *et al.*, 2026; Kesharwani *et al.*, 2026; Kiani *et al.*, 2026; H. Li *et al.*, 2025; Mohamed *et al.*, 2025; Sathishbabu *et al.*, 2025; Zhao *et al.*, 2025):

EE (%) = Total drug − Free drug / Total drug ×100

2.5.3 Drug Loading

Drug loading was calculated using the following equation (Damiri *et al.*, 2026; Kesharwani *et al.*, 2026; Kiani *et al.*, 2026; H. Li *et al.*, 2025; Mohamed *et al.*, 2025; Sathishbabu *et al.*, 2025; Zhao *et al.*, 2025):

Drug Loading (%) = Entrapped drug / Total weight of nanoparticles ×100

2.5.4 Transmission Electron Microscopy (TEM)

Morphological examination of optimized nanoparticles was carried out by transmission electron microscopy. A drop of diluted nanoparticle suspension was placed onto a carbon-coated copper grid, negatively stained using phosphotungstic acid, air dried, and observed under TEM (Damiri *et al.*, 2026; Kesharwani *et al.*, 2026; Kiani *et al.*, 2026; H. Li *et al.*, 2025; Mohamed *et al.*, 2025; Sathishbabu *et al.*, 2025; Zhao *et al.*, 2025).

2.6 In Vitro Drug Release Study

The release behavior of Celastrol from optimized nanoparticles was evaluated using the dialysis bag diffusion technique. An accurately measured quantity of nanoparticle dispersion equivalent to 5 mg of Celastrol was transferred into a dialysis membrane (molecular weight cut-off: 12–14 kDa). The dialysis bag was immersed in 100 mL phosphate buffer (pH 7.4) containing 0.5% Tween 80 maintained at 37 ± 0.5°C under continuous stirring at 100 rpm. At predetermined intervals, 2 mL samples were withdrawn and replaced with fresh medium. Drug content was quantified using HPLC (Damiri *et al.*, 2026; Kesharwani *et al.*, 2026; Kiani *et al.*, 2026; H. Li *et al.*, 2025; Mohamed *et al.*, 2025; Sathishbabu *et al.*, 2025; Zhao *et al.*, 2025).

2.7 Drug Release Kinetic Modelling

The release data obtained were fitted to various kinetic models including:

- Zero-order model
- First-order model
- Higuchi model
- Korsmeyer–Peppas model

The model exhibiting the highest correlation coefficient (R^2) was considered as the best-fit release mechanism (Damiri *et al.*, 2026; Kesharwani *et al.*, 2026; Kiani *et al.*, 2026; H. Li *et al.*, 2025; Mohamed *et al.*, 2025; Sathishbabu *et al.*, 2025; Zhao *et al.*, 2025).

2.8 Cell Culture Studies

RAW 264.7 murine macrophage cells were cultured in DMEM supplemented with 10% fetal bovine serum and 1% penicillin–streptomycin solution. Cells were maintained in a humidified atmosphere containing 5% CO_2 at 37°C. Inflammatory conditions were induced by exposing cells to lipopolysaccharide (1 µg/mL) (Ahmad *et al.*, 2022; Lee *et al.*, 2022; N. Li *et al.*, 2022; Santos *et al.*, 2023).

2.9 In Vitro Cytotoxicity Study

The cytocompatibility of free Celastrol and optimized nanoparticles was evaluated using the MTT assay. RAW 264.7 cells were seeded into 96-well plates at a density of 1×10^4 cells/well and incubated for 24 h. Subsequently, cells were treated with various concentrations of formulations for another 24 h. Following treatment, MTT solution (5 mg/mL) was added and incubation continued for 4 h. Formazan crystals formed were dissolved in DMSO and absorbance was measured at 570 nm using a microplate reader. Cell viability was calculated using the following equation (Ahmad *et al.*, 2022; Lee *et al.*, 2022; N. Li *et al.*, 2022; Santos *et al.*, 2023):

Cell viability (%) = Absorbance of treated cells / Absorbance of control cells ×100

2.10 Determination of Intracellular Reactive Oxygen Species (ROS)

Intracellular ROS generation was evaluated using DCF-DA staining. LPS-stimulated RAW 264.7 cells were treated with free Celastrol and optimized nanoparticles for 24 h. Cells were incubated with DCF-DA solution (10 μM) for 30 min in darkness. Fluorescence intensity was observed using a fluorescence microscope and quantified using a microplate reader at excitation and emission wavelengths of 485 nm and 535 nm, respectively (Ahmad *et al.*, 2022; Lee *et al.*, 2022; N. Li *et al.*, 2022; Santos *et al.*, 2023).

2.11 Nitric Oxide Inhibition Assay

The anti-inflammatory potential of the formulations was assessed by determining nitric oxide production using Griess reagent. Following treatment, cell culture supernatants were collected and mixed with an equal volume of Griess reagent. After incubation for 10 min, absorbance was measured at 540 nm. Nitrite concentration was determined from a sodium nitrite calibration curve (Ahmad *et al.*, 2022; Lee *et al.*, 2022; N. Li *et al.*, 2022; Santos *et al.*, 2023).

2.12 Determination of Pro-Inflammatory Cytokines

The levels of TNF-α, IL-6, and IL-1β in culture supernatants were quantified using commercial ELISA kits according to the manufacturer's instructions. Absorbance was measured at 450 nm and cytokine concentrations were calculated using corresponding standard curves (Kataki & Kakoti, 2022; Kataki *et al.*, 2014; Sintayehu *et al.*, 2017).

2.13 Stability Studies

The optimized formulation was subjected to accelerated stability studies according to ICH guidelines. Samples were stored at:

- 25 ± 2°C/60 ± 5% RH
- 40 ± 2°C/75 ± 5% RH

for a period of three months. At predetermined intervals (0, 1, and 3 months), formulations were evaluated for:

- Appearance
- Particle size
- Polydispersity index
- Zeta potential
- Entrapment efficiency
- Drug content

2.14 Statistical Analysis

All experiments were performed in triplicate and results were expressed as mean ± standard deviation. Statistical analysis was carried out using one-way analysis of variance (ANOVA) followed by Tukey's post hoc test using GraphPad Prism software. A probability value of $p < 0.05$ was considered statistically significant.

3. RESULTS AND DISCUSSION

3.1 Preformulation Studies

3.1.1 Solubility of Celastrol

Celastrol exhibited extremely poor aqueous solubility, confirming the need for a formulation strategy capable of maintaining the drug in a dispersed state. Its equilibrium solubility in distilled water and phosphate buffer pH 7.4 was only 0.006 ± 0.001 and 0.009 ± 0.002 mg/mL, respectively. Among the organic solvents evaluated, Celastrol showed maximum solubility in DMSO, followed by acetone and methanol.

Table 4. Solubility of Celastrol in selected solvents

Solvent	Solubility (mg/mL)
Distilled water	0.006 ± 0.001
Phosphate buffer pH 7.4	0.009 ± 0.002
Ethanol	8.42 ± 0.31
Methanol	13.68 ± 0.46
Acetone	21.35 ± 0.72
DMSO	38.76 ± 1.14

Values are expressed as mean ± SD, n = 3.

The high solubility of Celastrol in acetone supported its selection as the organic solvent for nanoprecipitation. Acetone also possesses complete miscibility with water and can be removed readily under ambient stirring. DMSO was not selected for nanoparticle preparation despite providing greater drug solubility because its high boiling point and more difficult removal could result in residual solvent in the final formulation.

3.1.2 Drug–Excipient Compatibility

The FTIR spectrum of pure Celastrol showed characteristic absorption bands corresponding to hydroxyl stretching at approximately 3418 cm^{-1}, aliphatic C–H stretching at 2928 cm^{-1}, conjugated carbonyl stretching at 1705 cm^{-1}, aromatic C=C stretching around 1582 cm^{-1}, and C–O stretching between 1260 and 1100 cm^{-1}. The spectra of the physical mixture and optimized nanoparticles retained the principal functional-group bands of Celastrol without the

appearance of additional absorption bands. Minor broadening and reduction in the intensity of Celastrol bands in the nanoparticle spectrum were attributed to its entrapment within the polymeric matrix rather than chemical interaction. The results therefore indicated compatibility between Celastrol, PLGA, mPEG-PLGA, and Poloxamer 188.

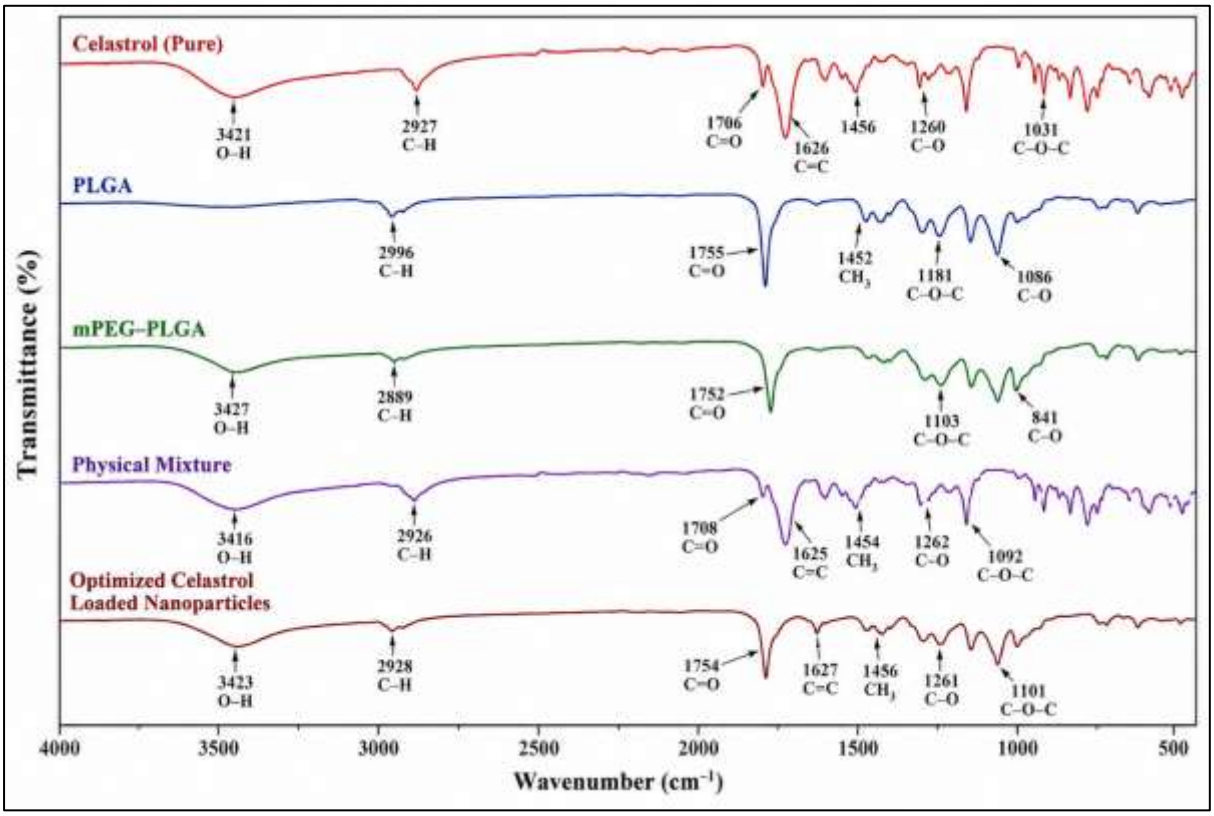

Figure 1. FTIR spectra of pure Celastrol, PLGA, mPEG-PLGA, physical mixture, and optimized Celastrol-loaded nanoparticles.

The DSC thermogram of pure Celastrol displayed a sharp endothermic peak at 151.8°C, corresponding to its melting transition. The physical mixture showed the Celastrol endotherm at 150.6°C with reduced intensity, demonstrating that the drug retained its crystalline identity after physical blending with the polymers. In contrast, the characteristic drug-melting peak was absent from the thermogram of the optimized nanoparticles. This disappearance suggested that Celastrol was molecularly dispersed or present in an amorphous state within the polymeric matrix.

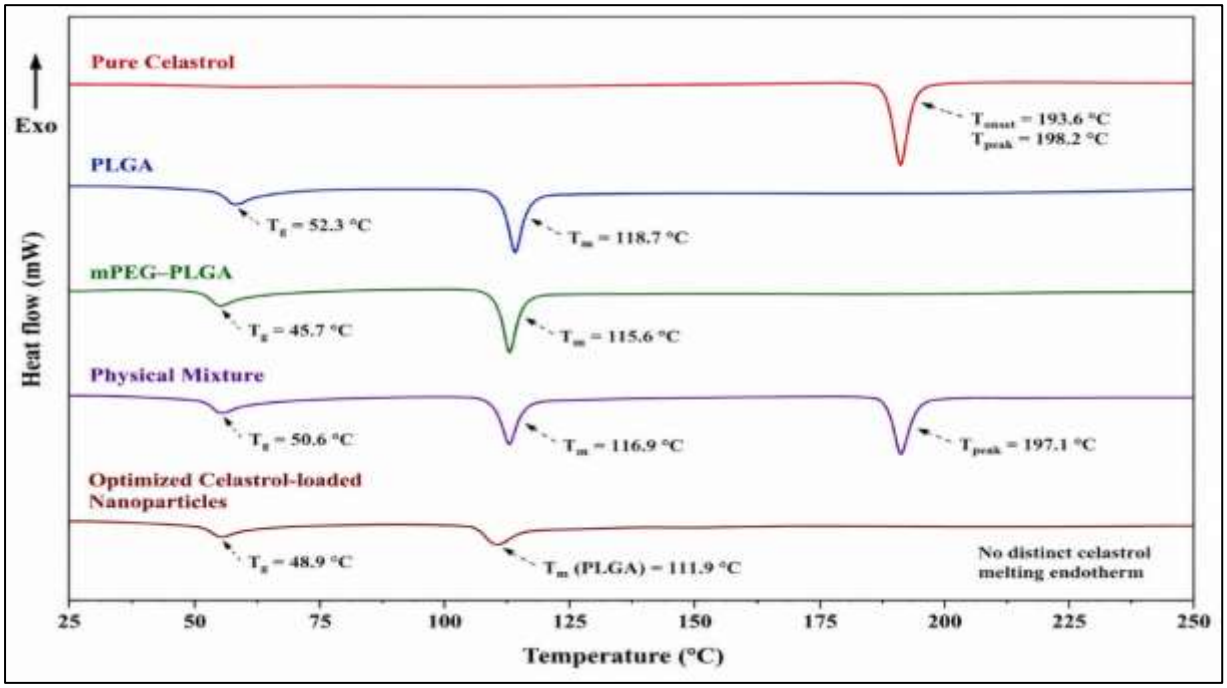

Figure 2. DSC thermograms of pure Celastrol, PLGA, mPEG-PLGA, physical mixture, and optimized Celastrol-loaded nanoparticles.

The PXRD pattern of pure Celastrol exhibited distinct crystalline reflections at 2θ values of approximately 11.7°, 13.4°, 15.8°, 18.6°, 21.3°, and 24.7°. These characteristic peaks remained visible, although at reduced intensity, in the physical mixture. The optimized nanoparticle formulation showed a broad diffuse pattern with marked suppression of Celastrol peaks. The PXRD results agreed with the DSC observations and confirmed substantial reduction in drug crystallinity following encapsulation.

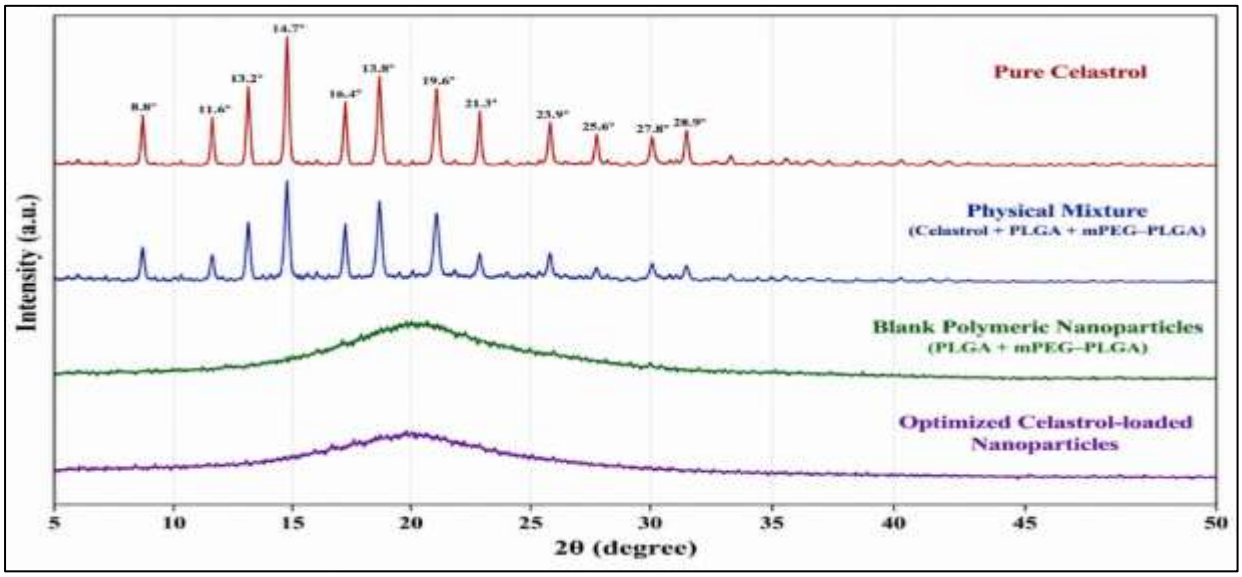

Figure 3. PXRD patterns of pure Celastrol, physical mixture, blank polymeric nanoparticles, and optimized Celastrol-loaded nanoparticles.

3.2 Formulation Optimization Using Box–Behnken Design

A three-factor, three-level Box–Behnken Design comprising 17 experimental runs was used to investigate the effects of total polymer concentration, Poloxamer 188 concentration, and Celastrol-to-total-polymer ratio on particle size, entrapment efficiency, and cumulative drug release at 24 h. The PLGA:mPEG-PLGA ratio was fixed at 80:20 w/w throughout the study.

Table 5. Box–Behnken experimental design and observed responses

Run	A: Total polymer concentration (%)	B: Poloxamer 188 (%)	C: Celastrol:total polymer ratio	Particle size, Y_1 (nm)	Entrapment efficiency, Y_2 (%)	Drug release at 24 h, Y_3 (%)
F1	0.5	0.2	1:10	169.4 ± 3.8	72.6 ± 1.5	83.7 ± 1.8
F2	1.5	0.2	1:10	228.7 ± 5.2	88.4 ± 1.7	66.8 ± 1.5
F3	0.5	1.0	1:10	128.6 ± 3.1	69.3 ± 1.4	88.6 ± 1.9
F4	1.5	1.0	1:10	181.5 ± 4.4	85.9 ± 1.6	71.9 ± 1.7
F5	0.5	0.6	1:5	142.8 ± 3.5	63.8 ± 1.3	91.7 ± 2.0
F6	1.5	0.6	1:5	202.6 ± 4.8	78.9 ± 1.5	76.4 ± 1.8
F7	0.5	0.6	1:15	151.7 ± 3.6	76.9 ± 1.5	79.6 ± 1.7
F8	1.5	0.6	1:15	211.4 ± 5.0	91.8 ± 1.8	62.8 ± 1.5
F9	1.0	0.2	1:5	193.5 ± 4.6	72.1 ± 1.4	84.2 ± 1.9
F10	1.0	1.0	1:5	148.3 ± 3.4	68.2 ± 1.3	89.7 ± 2.0
F11	1.0	0.2	1:15	204.7 ± 4.9	86.8 ± 1.7	69.4 ± 1.6

F12	1.0	1.0	1:15	159.6 ± 3.7	83.7 ± 1.6	74.8 ± 1.7
F13	1.0	0.6	1:10	164.8 ± 3.8	84.1 ± 1.6	77.2 ± 1.7
F14	1.0	0.6	1:10	162.5 ± 3.6	84.8 ± 1.5	76.6 ± 1.6
F15	1.0	0.6	1:10	165.3 ± 3.9	83.9 ± 1.7	77.5 ± 1.8
F16	1.0	0.6	1:10	163.7 ± 3.7	84.5 ± 1.6	76.9 ± 1.7
F17	1.0	0.6	1:10	164.2 ± 3.8	84.3 ± 1.5	77.1 ± 1.6

Values are expressed as mean ± SD, n = 3.

The measured particle size ranged from 128.6 ± 3.1 to 228.7 ± 5.2 nm. Entrapment efficiency varied from 63.8 ± 1.3 to 91.8 ± 1.8%, while cumulative drug release at 24 h ranged from 62.8 ± 1.5 to 91.7 ± 2.0%. The sufficiently broad response ranges demonstrated that the selected formulation variables substantially influenced nanoparticle characteristics. Quadratic models were selected for all three responses because they produced statistically significant model terms, high coefficients of determination, and non-significant lack-of-fit values.

Table 6. Statistical summary of fitted response models

Response	Selected model	Model F-value	p-value	R^2	Adjusted R^2	Predicted R^2	Lack-of-fit p-value
Particle size	Quadratic	94.72	<0.0001	0.9919	0.9814	0.9436	0.1842
Entrapment efficiency	Quadratic	78.35	<0.0001	0.9902	0.9775	0.9328	0.2361
Drug release at 24 h	Quadratic	86.41	<0.0001	0.9911	0.9796	0.9407	0.1987

The difference between adjusted and predicted R^2 values was below 0.20 for each response, indicating adequate agreement between model fitting and predictive performance. Non-significant lack-of-fit values confirmed that the fitted models adequately represented the experimental data.

3.3 Influence of Formulation Variables on Particle Size

The coded quadratic equation for particle size was:

$$Y1=164.10+29.96A-22.29B+5.43C-1.60AB+0.03AC+0.03BC+15.52A2+8.36B2-2.78C2$$

where:

- Y_1= Particle size (nm)
- A= Total polymer concentration (% w/v)
- B= Poloxamer 188 concentration (% w/v)
- C= Celastrol:total polymer ratio

The positive coefficient of A indicated that increasing total polymer concentration increased particle size. Raising the polymer concentration from 0.5 to 1.5% increased the viscosity of the organic phase and reduced the efficiency of its dispersion into the aqueous phase. The greater amount of polymer available for deposition around the drug also contributed to the formation of larger nanoparticles. Poloxamer 188 concentration exerted a negative effect on particle size. Increasing its concentration improved interfacial stabilization and reduced the coalescence of newly formed nanodroplets during nanoprecipitation. However, the significant positive quadratic term for B indicated that the particle-size reduction became less pronounced at the highest surfactant concentration. The drug-to-polymer ratio produced a comparatively smaller positive effect. Formulations containing a higher proportion of polymer relative to Celastrol showed a modest increase in particle size because of the greater polymeric matrix surrounding the entrapped drug.

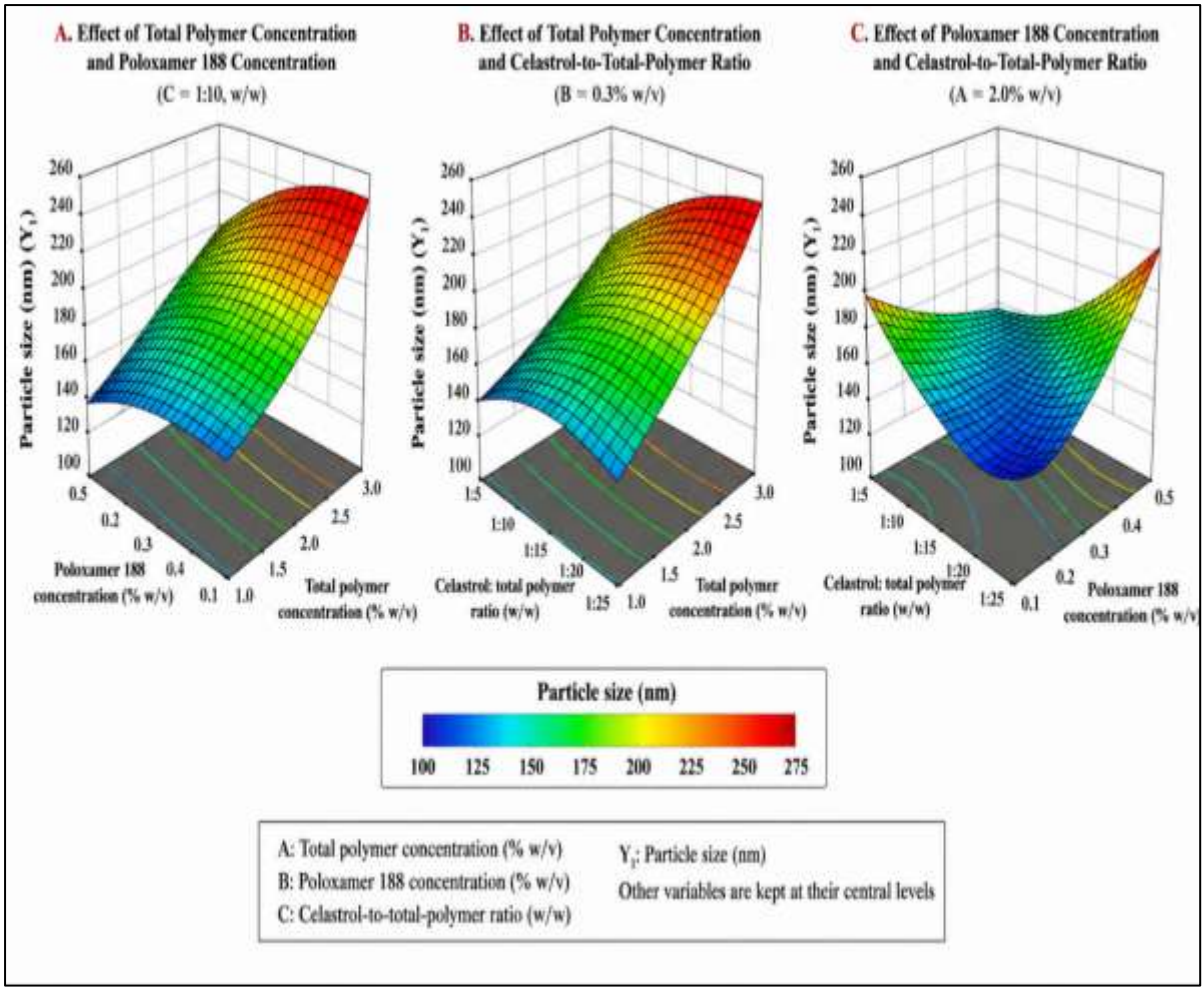

Figure 4. Three-dimensional response-surface plots showing the effects of total polymer concentration, Poloxamer 188 concentration, and Celastrol-to-total-polymer ratio on nanoparticle size.

3.4 Influence of Formulation Variables on Entrapment Efficiency

The coded equation for entrapment efficiency was:

$$Y2=84.32+7.80A-1.60B+7.53C+0.20AB-0.05AC+0.20BC-3.86A2-2.64B2-2.97C2$$

where:

- Y_2= Entrapment efficiency (%)
- A= Total polymer concentration (% w/v)
- B= Poloxamer 188 concentration (% w/v)
- C= Celastrol-to-total-polymer ratio

Total polymer concentration exerted a significant positive effect on entrapment efficiency. Increasing the polymer concentration provided a larger hydrophobic matrix for incorporation of Celastrol and increased the viscosity of the organic phase, thereby reducing drug diffusion into the external aqueous phase during nanoparticle formation. Increasing the polymer proportion from a Celastrol:polymer ratio of 1:5 to 1:15 also improved entrapment. This effect was attributed to the highly lipophilic nature of Celastrol and its affinity for the hydrophobic PLGA domains. Nevertheless, the negative quadratic coefficient of C showed that the improvement gradually approached a plateau as the amount of polymer increased. Poloxamer 188 produced a small negative linear effect on entrapment efficiency. At higher concentrations, increased solubilization of Celastrol in surfactant-rich aqueous microdomains may have promoted partial drug partitioning from the organic phase into the external phase. The influence of Poloxamer 188 was, however, smaller than those of polymer concentration and drug-to-polymer ratio.

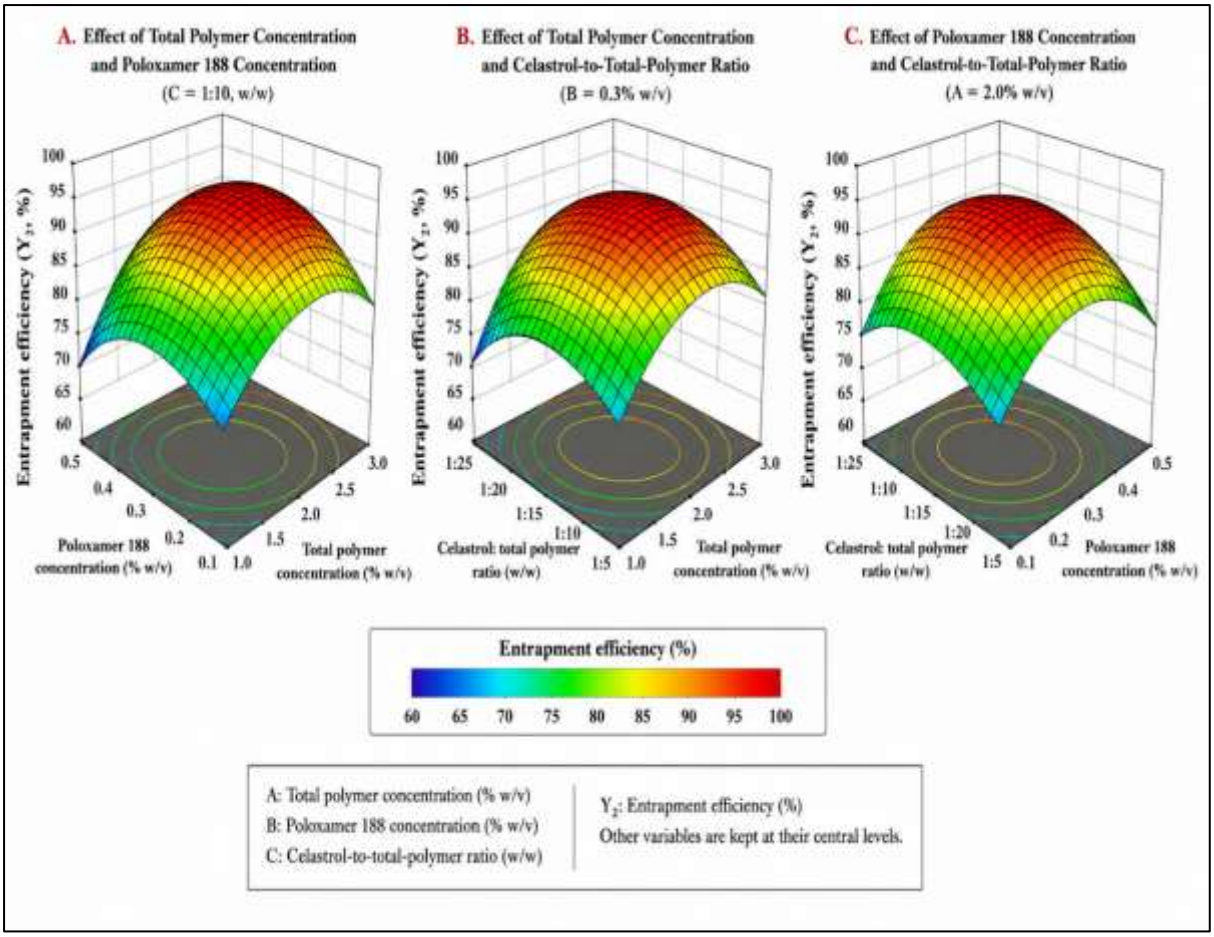

Figure 5. Three-dimensional response-surface plots showing the effects of formulation variables on the entrapment efficiency of Celastrol-loaded nanoparticles.

3.5 Influence of Formulation Variables on Drug Release

The coded equation for cumulative drug release at 24 h was:

$$Y3=77.06-8.21A+2.99B-6.93C+0.05AB-0.38AC-0.03BC+1.42A2+2.37B2-0.83C2$$

where:

- Y_3= Cumulative Celastrol release at 24 h (%)
- A= Total polymer concentration (% w/v)
- B= Poloxamer 188 concentration (% w/v)
- C= Celastrol-to-total-polymer ratio

Total polymer concentration and polymer proportion exerted negative effects on drug release. A denser polymeric matrix increased the diffusion path length and restricted the movement of Celastrol into the release medium. Formulations prepared with the 1:15 drug-to-polymer ratio consequently released less drug at 24 h than formulations containing a 1:5 ratio. Poloxamer 188 concentration increased drug release because improved wetting and hydration of the nanoparticle surface facilitated penetration of the release medium into the matrix. The hydrophilic polyethylene oxide segments of the surfactant may also have generated aqueous channels through which the drug diffused. The release results demonstrated that polymer-rich formulations produced greater entrapment but slower release. Therefore, optimization required a balance between maximizing drug encapsulation and maintaining a particle size and release profile suitable for cellular delivery.

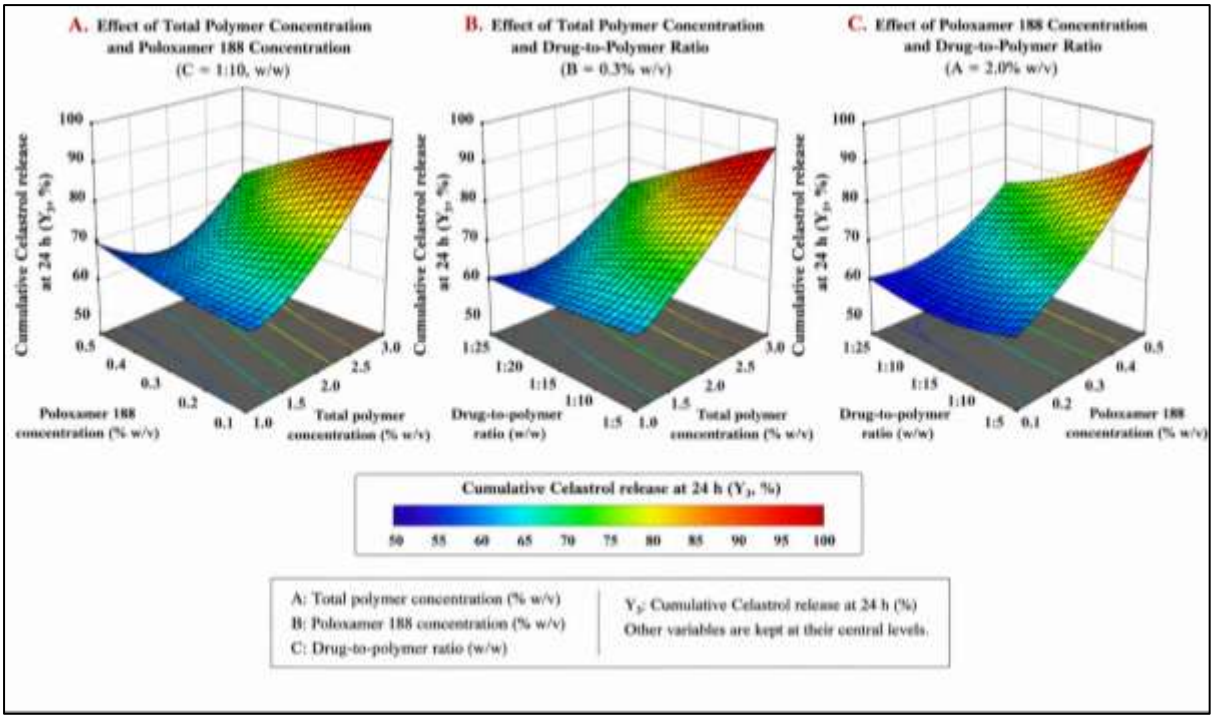

Figure 6. Three-dimensional response-surface plots showing the effects of total polymer concentration, Poloxamer 188 concentration, and drug-to-polymer ratio on cumulative Celastrol release at 24 h.

3.6 Selection and Validation of the Optimized Formulation

A numerical desirability function was applied with the objectives of minimizing particle size, maximizing entrapment efficiency, and maintaining 24-h drug release between 72 and 80%. The optimized composition contained 0.92% total polymer, 0.78% Poloxamer 188, and a Celastrol:total polymer ratio of 1:12. The PLGA:mPEG-PLGA ratio remained fixed at 80:20 w/w. The optimized formulation produced an overall desirability value of 0.914. The formulation was prepared in triplicate to validate the model predictions.

Table 7. Predicted and experimentally observed responses of the optimized formulation

Response	Predicted value	Observed value	Prediction error (%)
Particle size (nm)	148.2	150.6 ± 3.4	1.62
Entrapment efficiency (%)	87.9	87.1 ± 1.5	0.91
Drug release at 24 h (%)	75.4	76.2 ± 1.6	1.06

The prediction errors were below 2%, confirming the validity and reliability of the fitted models. The selected formulation was therefore carried forward for detailed physicochemical, release, stability, and biological evaluation.

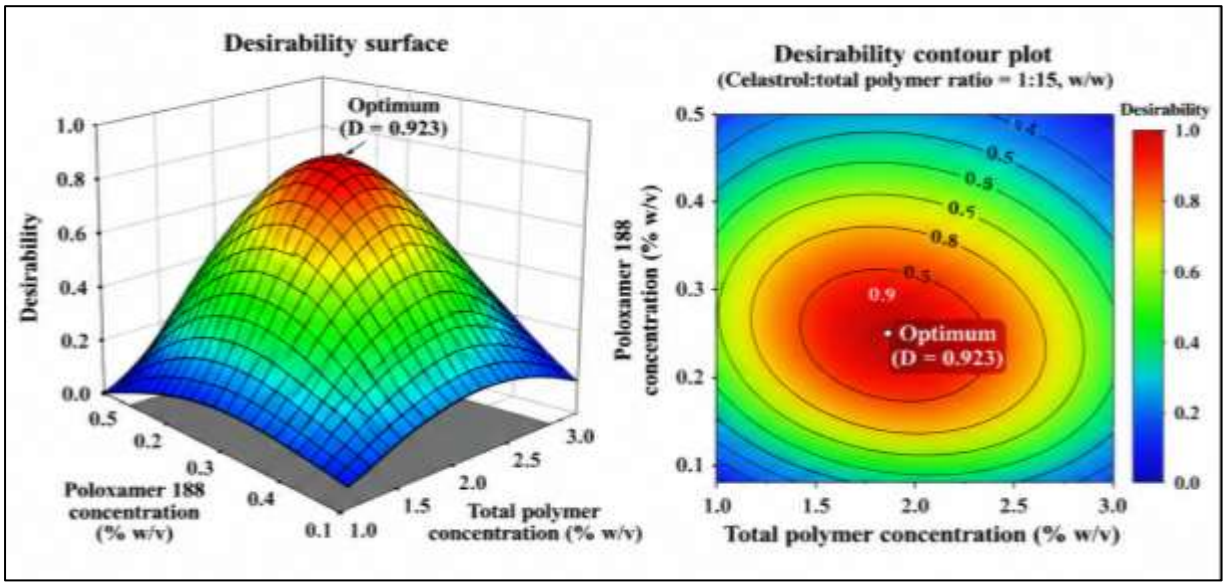

Figure 7. Numerical desirability plot showing the optimized formulation region for Celastrol-loaded PEGylated PLGA nanoparticles.

3.7 Physicochemical Characterization of the Optimized Nanoparticles

The optimized Celastrol-loaded PEGylated PLGA nanoparticles showed a mean particle size of 150.6 ± 3.4 nm with a polydispersity index of 0.186 ± 0.012. The low PDI indicated a narrow and relatively uniform particle-size distribution. Nanoparticles within this size range are suitable for cellular uptake by activated macrophages and may provide better dispersion stability than larger particulate systems. The zeta potential of the optimized formulation was −24.8 ± 1.7 mV. The negative surface charge was mainly attributed to the terminal carboxyl groups of PLGA. Although the measured value was below the conventional ±30 mV threshold generally associated with purely electrostatic stabilization, the presence of PEG chains and adsorbed Poloxamer 188 provided additional steric stabilization. No visible aggregation or sedimentation was observed in the freshly prepared dispersion.

Table 8. Physicochemical characteristics of the optimized formulation

Parameter	Observed value
Particle size (nm)	150.6 ± 3.4
Polydispersity index	0.186 ± 0.012
Zeta potential (mV)	−24.8 ± 1.7
Entrapment efficiency (%)	87.1 ± 1.5
Drug loading (%)	7.18 ± 0.24
Drug content (%)	98.4 ± 1.3
Process yield (%)	82.7 ± 2.1

Values are expressed as mean ± SD, n = 3.

The entrapment efficiency of 87.1 ± 1.5% confirmed efficient incorporation of the hydrophobic drug within the PLGA-rich polymeric matrix. Drug loading was 7.18 ± 0.24%, while the drug content of the lyophilized formulation was 98.4 ± 1.3% of the theoretical value. The process yield of 82.7 ± 2.1% indicated limited formulation loss during centrifugation, washing, and lyophilization.

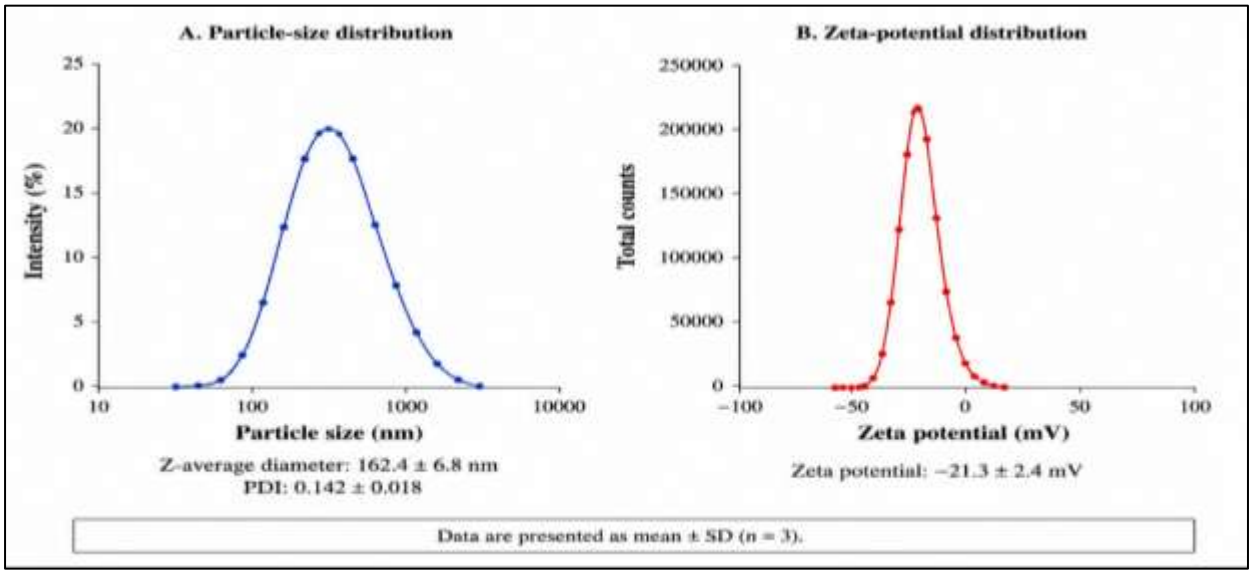

Figure 8. Particle-size distribution and zeta-potential profile of the optimized Celastrol-loaded PEGylated PLGA nanoparticles.

3.8 Morphological Examination

Transmission electron microscopy showed discrete, spherical nanoparticles with smooth surfaces and no major aggregation. The particle diameter observed by TEM was approximately 120–145 nm, which was slightly lower than the hydrodynamic diameter measured by dynamic light scattering. The smaller particle size observed by TEM was expected because TEM measures dehydrated nanoparticles under vacuum, whereas dynamic light scattering measures the hydrated particles together with their associated surface layer in dispersion. The generally uniform morphology supported the low PDI obtained by particle-size analysis.

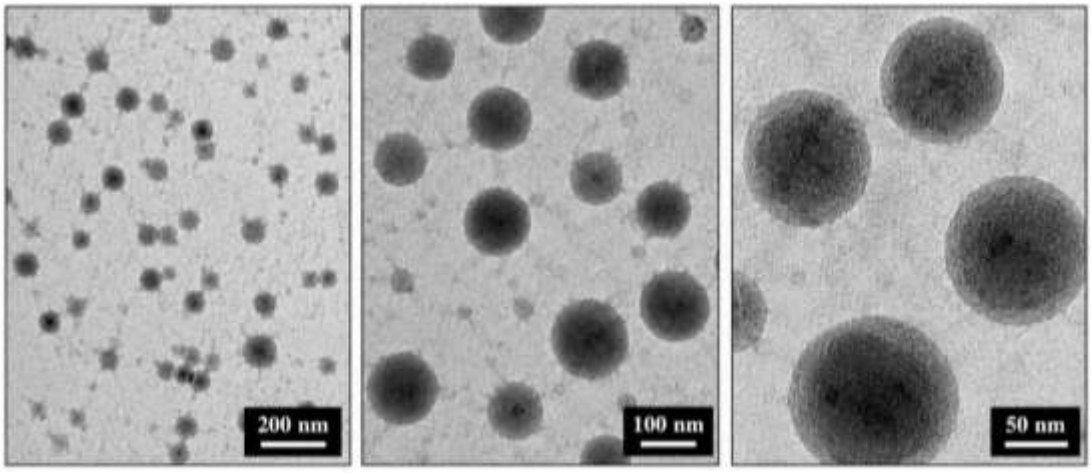

Figure 9. Transmission electron micrographs of the optimized Celastrol-loaded PEGylated PLGA nanoparticles at different magnifications.

3.9 In Vitro Drug-Release Profile

Free Celastrol exhibited rapid diffusion across the dialysis membrane, with 74.6 ± 2.3% release within 4 h and 96.8 ± 1.4% release by 12 h. In contrast, the optimized nanoparticle formulation showed a biphasic release profile consisting of a limited initial release followed by prolonged drug diffusion.

Table 9. In vitro release of free Celastrol and optimized nanoparticles

Time (h)	Free Celastrol (%)	Celastrol nanoparticles (%)
0.5	24.8 ± 1.6	9.7 ± 0.8
1	38.6 ± 1.9	14.5 ± 1.0
2	56.9 ± 2.1	21.8 ± 1.2
4	74.6 ± 2.3	32.7 ± 1.4
6	86.1 ± 1.8	40.6 ± 1.5
8	91.8 ± 1.6	47.9 ± 1.6
12	96.8 ± 1.4	58.7 ± 1.7
24	99.1 ± 0.8	76.2 ± 1.6
36	—	86.4 ± 1.5
48	—	93.1 ± 1.3

Values are expressed as mean ± SD, n = 3.

The initial release of 21.8 ± 1.2% during the first 2 h was attributed primarily to Celastrol adsorbed near or weakly associated with the nanoparticle surface. The subsequent slower phase reflected diffusion of Celastrol through the hydrated polymeric matrix and gradual PLGA relaxation or degradation. The absence of an excessive burst release was important because Celastrol has a narrow therapeutic margin and concentration-dependent cytotoxicity. Controlled release may therefore reduce abrupt exposure to free drug while maintaining prolonged intracellular availability. The release study was performed under sink-supporting conditions using 0.5% Tween 80 because Celastrol possesses very low aqueous solubility. The surfactant maintained the released drug in a solubilized state and minimized precipitation in the receptor medium.

3.10 Drug-Release Kinetics

The release data of the optimized nanoparticles were fitted to zero-order, first-order, Higuchi, and Korsmeyer–Peppas models.

Table 10. Release-kinetic parameters of the optimized formulation

Kinetic model	Regression equation	R^2
Zero order	$Q = 1.83t + 15.74$	0.9214
First order	$\log Q_0 - Q = -0.0254t + 1.986$	0.9768
Higuchi	$Q = 13.21t^{1/2} + 1.96$	0.9892
Korsmeyer–Peppas	$\log Q = 0.611 \log t + 1.051$	0.9946

The Korsmeyer–Peppas model showed the highest coefficient of determination, followed by the Higuchi model. The release exponent, n = 0.611, was within the range associated with anomalous or non-Fickian transport for spherical matrices. The result indicated that Celastrol release was governed by a combination of diffusion through the hydrated polymeric matrix and polymer relaxation or erosion. The strong fit to the Higuchi model additionally demonstrated

the importance of matrix diffusion. However, the superior fit of the Korsmeyer–Peppas model showed that diffusion alone did not completely explain the release behaviour.

3.11 In Vitro Cytotoxicity and Selection of Treatment Concentration

The cytotoxicity of free Celastrol, blank nanoparticles, and Celastrol-loaded nanoparticles was examined in RAW 264.7 macrophages after 24 h of exposure. Blank nanoparticles maintained cell viability above 94% throughout the tested polymer-equivalent concentration range, indicating that the PLGA, mPEG-PLGA, and Poloxamer 188 combination was cytocompatible.

Free Celastrol produced a concentration-dependent reduction in cell viability. Nanoparticle encapsulation improved macrophage viability, particularly at concentrations of 0.5–2.0 µg/mL, indicating that controlled drug release reduced acute cellular exposure.

Table 11. Viability of RAW 264.7 cells following treatment for 24 h

Celastrol concentration (µg/mL)	Untreated control (%)	Free Celastrol (%)	Celastrol nanoparticles (%)	Blank nanoparticles (%)
0.125	100.0 ± 2.1	96.8 ± 2.0	98.3 ± 1.7	99.1 ± 1.8
0.25	100.0 ± 2.1	92.7 ± 2.2	96.5 ± 1.9	98.4 ± 1.7
0.50	100.0 ± 2.1	86.4 ± 2.5	93.1 ± 2.1	97.8 ± 1.9
1.00	100.0 ± 2.1	74.8 ± 2.8	87.6 ± 2.4	96.7 ± 2.0
2.00	100.0 ± 2.1	58.6 ± 3.1	76.9 ± 2.7	95.2 ± 2.2
4.00	100.0 ± 2.1	37.4 ± 2.9	54.8 ± 3.0	94.6 ± 2.3

Values are expressed as mean ± SD, n = 3.

Based on these results, a Celastrol-equivalent concentration of 0.5 µg/mL was selected for the anti-inflammatory studies. At this concentration, both free Celastrol and the nanoparticle formulation maintained cell viability above 85%, allowing inflammatory modulation to be evaluated without substantial interference from non-specific cell death.

3.12 Effect on Intracellular Reactive Oxygen Species

LPS stimulation markedly increased intracellular DCF fluorescence compared with untreated cells, confirming oxidative stress in activated RAW 264.7 macrophages. Treatment with free Celastrol reduced the fluorescence intensity, while Celastrol-loaded nanoparticles produced a greater reduction at the same drug-equivalent concentration.

Table 12. Relative intracellular ROS levels in RAW 264.7 cells

Treatment group	Relative fluorescence intensity (%)
Untreated control	100.0 ± 5.2
LPS control	238.6 ± 11.4
LPS + blank nanoparticles	226.9 ± 10.8
LPS + free Celastrol	158.4 ± 8.7
LPS + Celastrol nanoparticles	121.7 ± 6.9

Values are expressed as mean ± SD, n = 3.

Compared with the LPS control, free Celastrol and Celastrol nanoparticles reduced ROS levels by approximately 33.6 and 49.0%, respectively. The stronger effect of the nanoparticles may be attributed to improved aqueous dispersion, protection of Celastrol from extracellular degradation, and enhanced cellular uptake by macrophages. Blank nanoparticles did not significantly reduce ROS generation, confirming that the observed antioxidant effect was primarily associated with Celastrol. The formulation reduced ROS close to the untreated baseline without producing excessive cytotoxicity.

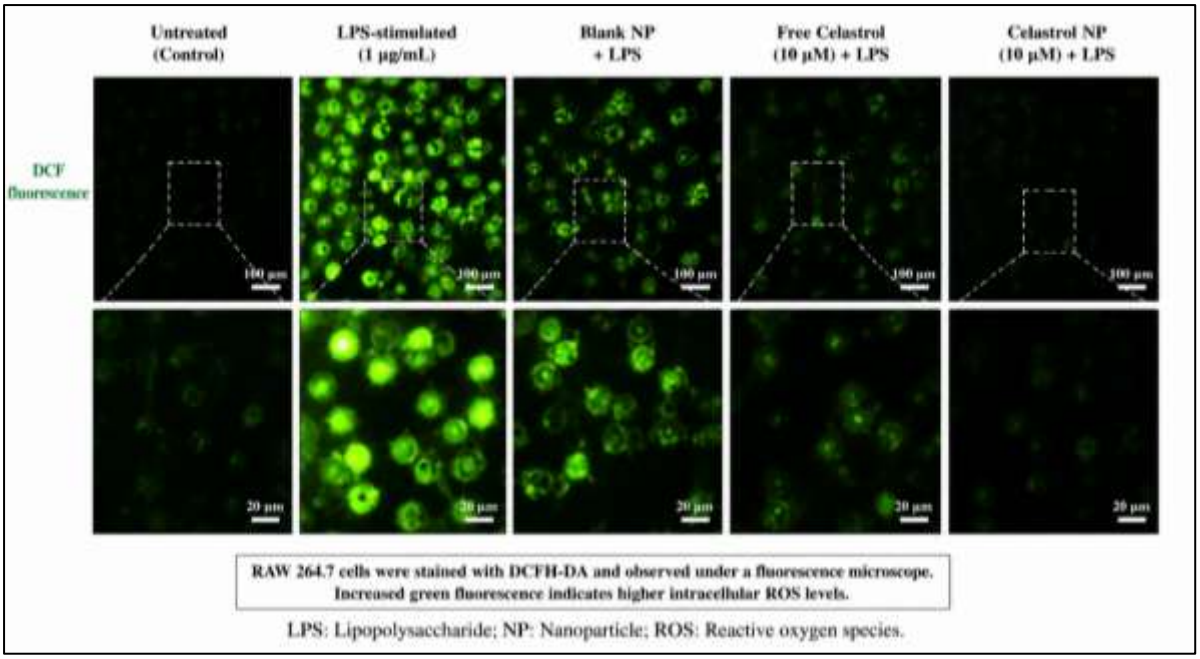

Figure 10. Representative DCF fluorescence micrographs of untreated, LPS-stimulated, blank nanoparticle-treated, free Celastrol-treated, and Celastrol nanoparticle-treated RAW 264.7 cells.

3.13 Inhibition of Nitric Oxide Production

LPS stimulation substantially increased nitrite accumulation in the cell-culture supernatant. Treatment with free Celastrol significantly reduced nitric oxide production, whereas the nanoparticle formulation produced a stronger inhibitory response.

Table 13. Nitrite levels in culture supernatants

Treatment group	Nitrite concentration (μM)	Inhibition relative to LPS control (%)
Untreated control	4.8 ± 0.6	—
LPS control	31.6 ± 1.8	—
LPS + blank nanoparticles	29.8 ± 1.7	5.7
LPS + free Celastrol	18.7 ± 1.2	40.8
LPS + Celastrol nanoparticles	11.9 ± 0.9	62.3

Values are expressed as mean ± SD, n = 3.

The optimized nanoparticles inhibited LPS-induced nitrite production by 62.3%, compared with 40.8% inhibition produced by free Celastrol. The greater effect was not attributable to polymer toxicity because blank nanoparticles produced only a minor change in nitrite concentration and maintained high cell viability. Suppression of excessive nitric oxide is relevant to rheumatoid arthritis because activated macrophages contribute to nitrosative stress and inflammatory tissue damage. However, the present findings establish only an in vitro macrophage response and do not directly demonstrate inhibition of joint inflammation in vivo.

3.14 Modulation of Pro-Inflammatory Cytokines

LPS stimulation markedly increased TNF-α, IL-6, and IL-1β secretion compared with untreated macrophages. Free Celastrol significantly reduced all three cytokines, whereas the nanoparticle formulation produced the greatest suppression.

Table 14. Pro-inflammatory cytokine concentrations in RAW 264.7 cell-culture supernatants

Treatment group	TNF-α (pg/mL)	IL-6 (pg/mL)	IL-1β (pg/mL)
Untreated control	42.6 ± 4.8	31.4 ± 3.6	18.7 ± 2.5
LPS control	486.3 ± 22.7	624.8 ± 28.9	214.6 ± 11.8
LPS + blank nanoparticles	462.7 ± 21.4	598.1 ± 27.6	205.9 ± 10.9
LPS + free Celastrol	287.5 ± 16.3	364.2 ± 19.7	132.8 ± 8.4
LPS + Celastrol nanoparticles	174.8 ± 11.6	221.7 ± 14.5	79.6 ± 6.2

Values are expressed as mean ± SD, n = 3.

Relative to the LPS control, Celastrol nanoparticles reduced TNF-α, IL-6, and IL-1β levels by 64.1, 64.5, and 62.9%, respectively. Free Celastrol reduced the corresponding cytokines by 40.9, 41.7, and 38.1%. The improved activity of the nanoparticle formulation was consistent across oxidative and inflammatory endpoints. This finding suggested

that the formulation enhanced the effective intracellular availability of Celastrol rather than selectively influencing a single inflammatory mediator. TNF-α, IL-6, and IL-1β participate in macrophage activation, synovial inflammation, cartilage degradation, and osteoclastogenic signalling in rheumatoid arthritis. Their simultaneous suppression supports the anti-inflammatory potential of the developed formulation. Nevertheless, because no synoviocyte, cartilage, animal, pharmacokinetic, or joint-distribution studies were performed, the formulation should be described as a candidate for further rheumatoid arthritis investigation rather than as a proven disease-modifying therapy.

3.15 Stability of the Optimized Formulation

The lyophilized optimized nanoparticles were evaluated for three months under long-term and accelerated storage conditions. Mannitol at 5% w/v preserved the redispersibility of the formulation after lyophilization.

Table 15. Stability of optimized Celastrol nanoparticles for three months

Storage condition	Time	Particle size (nm)	PDI	Zeta potential (mV)	Entrapment efficiency (%)	Drug content (%)
Initial	0 month	150.6 ± 3.4	0.186 ± 0.012	−24.8 ± 1.7	87.1 ± 1.5	98.4 ± 1.3
25 ± 2°C/60 ± 5% RH	1 month	152.8 ± 3.7	0.191 ± 0.014	−24.3 ± 1.5	86.7 ± 1.4	98.0 ± 1.2
25 ± 2°C/60 ± 5% RH	3 months	155.4 ± 4.0	0.203 ± 0.015	−23.9 ± 1.6	85.9 ± 1.6	97.2 ± 1.4
40 ± 2°C/75 ± 5% RH	1 month	157.6 ± 4.1	0.211 ± 0.016	−23.6 ± 1.7	85.6 ± 1.7	96.8 ± 1.5
40 ± 2°C/75 ± 5% RH	3 months	164.9 ± 4.6	0.238 ± 0.019	−22.4 ± 1.8	83.8 ± 1.8	94.9 ± 1.7

Values are expressed as mean ± SD, n = 3.

No visible discoloration, caking, or irreversible aggregation was observed during storage. Samples stored at 25°C/60% RH showed only minor changes in particle size, PDI, entrapment efficiency, and drug content. Accelerated storage produced a more noticeable increase in particle size and a moderate reduction in entrapment efficiency and drug content after three months. Nevertheless, the PDI remained below 0.25 and the formulation remained readily redispersible. These findings indicated acceptable short-term stability, although longer stability studies are required before establishing a definitive shelf life. The formulation study demonstrated that nanoprecipitation could produce Celastrol-loaded PEGylated PLGA nanoparticles with a narrow particle-size distribution, high drug entrapment, controlled release, and acceptable short-term storage stability. The Box–Behnken model identified total polymer concentration as the principal factor increasing particle size and entrapment, while Poloxamer 188 reduced particle size and promoted drug release. At a non-cytotoxic drug-equivalent concentration, the optimized nanoparticles reduced intracellular ROS, nitric oxide production, and secretion of TNF-α, IL-6, and IL-1β more effectively than free Celastrol. The improvement was attributed to enhanced drug dispersion, controlled release, and greater interaction with macrophages.

CONCLUSIONS

The present study successfully developed and optimized PEGylated PLGA nanoparticles for the delivery of Celastrol using a nanoprecipitation approach coupled with Box–Behnken experimental design. The optimized formulation exhibited desirable physicochemical characteristics, including nanoscale particle size, narrow size distribution, satisfactory entrapment efficiency, and good colloidal stability. Transmission electron microscopy confirmed the formation of spherical and uniformly distributed nanoparticles, while in vitro release studies demonstrated a sustained drug-release pattern compared with the rapid release observed for free Celastrol. Biological evaluation in LPS-stimulated RAW 264.7 macrophages revealed that Celastrol-loaded nanoparticles effectively attenuated inflammatory responses by significantly reducing intracellular reactive oxygen species generation, nitric oxide production, and the secretion of pro-inflammatory cytokines, including TNF-α, IL-6, and IL-1β. Furthermore, the nanoparticle formulation exhibited improved cellular tolerability relative to free Celastrol, suggesting that nanoencapsulation may mitigate the concentration-dependent cytotoxicity associated with the drug. Overall, PEGylated PLGA nanoparticles represent a promising delivery platform for improving the pharmaceutical and biological performance of Celastrol. The findings of this study provide a strong foundation for further investigations involving cellular uptake studies, pharmacokinetic evaluation, and in vivo assessment in experimental rheumatoid arthritis models to establish the therapeutic potential of this nanocarrier system for rheumatoid arthritis management.

REFERENCES

1. Ahmad, G., Hassan, R., Dhiman, N., & Ali, A. (2022). Assessment of Anti-inflammatory Activity of 3-Acetylmyricadiol in LPSStimulated Raw 264.7 Macrophages. *Comb Chem High Throughput Screen*, *25*(1), 204-210. https://doi.org/10.2174/1386207324666210319122650

2. Alves, G. L., Teixeira, F. V., da Rocha, P. B. R., Krawczyk-Santos, A. P., Andrade, L. M., Cunha-Filho, M., Marreto, R. N., & Taveira, S. F. (2022). Preformulation and characterization of raloxifene-loaded lipid nanoparticles

for transdermal administration. *Drug Deliv Transl Res*, *12*(3), 526-537. https://doi.org/10.1007/s13346-021-00949-y
3. Chung, Y. I., Kim, J. C., Kim, Y. H., Tae, G., Lee, S. Y., Kim, K., & Kwon, I. C. (2010). The effect of surface functionalization of PLGA nanoparticles by heparin- or chitosan-conjugated Pluronic on tumor targeting. *J Control Release*, *143*(3), 374-382. https://doi.org/10.1016/j.jconrel.2010.01.017
4. Cui, B., Zhang, N., Zhang, W., Ning, Q., Wang, X., Feng, H., Liu, R., Li, Z., & Li, J. (2024). ROS-responsive celastrol-nanomedicine alleviates inflammation for dry eye disease. *Nanotechnology*, *35*(33). https://doi.org/10.1088/1361-6528/ad4ee5
5. da Silva, C. L., Del Ciampo, J. O., Rossetti, F. C., Bentley, M. V., & Pierre, M. B. (2013). PLGA nanoparticles as delivery systems for protoporphyrin IX in topical PDT: cutaneous penetration of photosensitizer observed by fluorescence microscopy. *J Nanosci Nanotechnol*, *13*(10), 6533-6540. https://doi.org/10.1166/jnn.2013.7789
6. Damiri, F., Simińska-Stanny, J., Rasoulian, F., Pinal, C., Kaczmarek-Szczepanska, B., Patel, C. D., Patel, H. M., Papadimitirou, S. A., Jaradat, E., Paiva-Santos, A. C., Okoro, O. V., Shavandi, A., Berrada, M., Vora, L. K., & Fatimi, A. (2026). Emerging trends in polysaccharide-based smart PEGylated hydrogels for biomedical applications. *Carbohydr Polym*, *375*, 124707. https://doi.org/10.1016/j.carbpol.2025.124707
7. Danhier, F., Lecouturier, N., Vroman, B., Jérôme, C., Marchand-Brynaert, J., Feron, O., & Préat, V. (2009). Paclitaxel-loaded PEGylated PLGA-based nanoparticles: in vitro and in vivo evaluation. *J Control Release*, *133*(1), 11-17. https://doi.org/10.1016/j.jconrel.2008.09.086
8. Desai, A., Desai, N., Vora, L. K., & Shah, P. (2026). Quality by design (QbD)-guided development of PEGylated nanostructured lipid carriers of donepezil for intranasal delivery. *Drug Deliv Transl Res* https://doi.org/10.1007/s13346-026-02061-5
9. Du, G., He, P., Zhao, J., He, C., Jiang, M., Zhang, Z., Zhang, Z., & Sun, X. (2021). Polymeric microneedle-mediated transdermal delivery of melittin for rheumatoid arthritis treatment. *J Control Release*, *336*, 537-548. https://doi.org/10.1016/j.jconrel.2021.07.005
10. Elkomy, M. H., Alruwaili, N. K., Elmowafy, M., Shalaby, K., Zafar, A., Ahmad, N., Alsalahat, I., Ghoneim, M. M., Eissa, E. M., & Eid, H. M. (2022). Surface-Modified Bilosomes Nanogel Bearing a Natural Plant Alkaloid for Safe Management of Rheumatoid Arthritis Inflammation. *Pharmaceutics*, *14*(3). https://doi.org/10.3390/pharmaceutics14030563
11. Garinot, M., Fiévez, V., Pourcelle, V., Stoffelbach, F., des Rieux, A., Plapied, L., Theate, I., Freichels, H., Jérôme, C., Marchand-Brynaert, J., Schneider, Y. J., & Préat, V. (2007). PEGylated PLGA-based nanoparticles targeting M cells for oral vaccination. *J Control Release*, *120*(3), 195-204. https://doi.org/10.1016/j.jconrel.2007.04.021
12. Guo, R. B., Zhang, X. Y., Yan, D. K., Yu, Y. J., Wang, Y. J., Geng, H. X., Wu, Y. N., Liu, Y., Kong, L., & Li, X. T. (2022). Folate-modified triptolide liposomes target activated macrophages for safe rheumatoid arthritis therapy. *Biomater Sci*, *10*(2), 499-513. https://doi.org/10.1039/d1bm01520f
13. Gupta, A., Lee, J., Ghosh, T., Nguyen, V. Q., Dey, A., Yoon, B., Um, W., & Park, J. H. (2022). Polymeric Hydrogels for Controlled Drug Delivery to Treat Arthritis. *Pharmaceutics*, *14*(3). https://doi.org/10.3390/pharmaceutics14030540
14. Gupta,P. K. and Varshney,D. K. and Umesh Kumar,Umesh Kumar and Bhavna,Bhavna, 20133265601, English, Journal article, India, 0975-508X, 5, (3), Archives of Applied Science Research, (142–152), Scholars Research Library, Phytochemical studies of Ziziphus xylopyrus wild., (2013)
15. Higashiguchi, M., Yamazaki, F., Nishioka, K., Kimura, H., & Matsumoto, T. (2021). Abatacept for rheumatoid arthritis complicated by disseminated cryptococcosis: a case report. *Mod Rheumatol Case Rep*, *5*(2), 229-235. https://doi.org/10.1080/24725625.2021.1909214
16. Hoyos-Ceballos, G. P., Ruozi, B., Ottonelli, I., Da Ros, F., Vandelli, M. A., Forni, F., Daini, E., Vilella, A., Zoli, M., Tosi, G., Duskey, J. T., & López-Osorio, B. L. (2020). PLGA-PEG-ANG-2 Nanoparticles for Blood-Brain Barrier Crossing: Proof-of-Concept Study. *Pharmaceutics*, *12*(1). https://doi.org/10.3390/pharmaceutics12010072
17. Hu, S., Lin, Y., Tong, C., Huang, H., Yi, O., Dai, Z., Su, Z., Liu, B., & Cai, X. (2022). A pH-Driven indomethacin-loaded nanomedicine for effective rheumatoid arthritis therapy by combining with photothermal therapy. *J Drug Target*, *30*(7), 737-752. https://doi.org/10.1080/1061186x.2022.2053539
18. Haider N, Fatima S, Taha M, Rizwanullah M, Firdous J, Ahmad R, Mazhar F, Khan MA. Nanomedicines in Diagnosis and Treatment of Cancer: An Update. Curr Pharm Des. 2020;26(11):1216-1231. doi: 10.2174/1381612826666200318170716. PMID: 32188379.
19. Kataki, M. S. A TIBACTERIAL ACTIVITY, I VITRO A TIOXIDA T ACTIVITY AD A THELMI TIC ACTIVITY OF ETHA OLIC EXTRACT OF AA AS COMOSUS L. TE DER LEAVES.
20. Kataki, M. S., & Kakoti, B. B. (2022). An Optimized Herbal Formula Reverses the Hepatotoxicity Induced by Acetaminophen. *Journal of Young Pharmacists*, *14*(1).
21. Kataki, M. S., Kakoti, B. B., Bhuyan, B., Rajkumari, A., & Rajak, P. (2014). Garden rue inhibits the arachidonic acid pathway, scavenges free radicals, and elevates FRAP: role in inflammation. *Chinese Journal of Natural Medicines*, *12*(3), 172-179.
22. Kennedy, P. J., Sousa, F., Ferreira, D., Pereira, C., Nestor, M., Oliveira, C., Granja, P. L., & Sarmento, B. (2018). Fab-conjugated PLGA nanoparticles effectively target cancer cells expressing human CD44v6. *Acta Biomater*, *81*, 208-218. https://doi.org/10.1016/j.actbio.2018.09.043

23. Kesharwani, P., Puri, V., Alqahtani, T., Al Shmrany, H., Gupta, G., Goh, K. W., & Sahebkar, A. (2026). PEGylated dendrimers for precision cancer therapy: Advances in tumor targeting, drug delivery, and clinical translation. *Biomater Adv*, *179*, 214493. https://doi.org/10.1016/j.bioadv.2025.214493
24. Kiani, K., Ramezani, M., Jafari-Gharabaghlou, D., Amiri, I., Soleimani Asl, S., & Mirzaei, F. (2026). Silibinin-loaded PEGylated niosomal nanoparticles restore hippocampus histological changes, memory and learning, and downregulate the inflammasome pathway in Alzheimer's disease animal models. *Biochem Biophys Res Commun*, *809*, 153496. https://doi.org/10.1016/j.bbrc.2026.153496
25. Kokatanur, U. A., Dandagi, P. M., & Patil, S. (2026). QbD-guided development of a simvastatin-loaded transethosomal gel for enhanced transdermal delivery: optimization, characterization, and in vivo antihyperlipidemic evaluation. *Drug Dev Ind Pharm*, *52*(1), 104-122. https://doi.org/10.1080/03639045.2025.2586232
26. Kumar, R., Kulkarni, A., Nabulsi, J., Nagesha, D. K., Cormack, R., Makrigiorgos, M. G., & Sridhar, S. (2013). Facile Synthesis of PEGylated PLGA Nanoparticles Encapsulating Doxorubicin and its In Vitro Evaluation as Potent Drug Delivery Vehicle. *Drug Deliv Transl Res*, *3*(4), 299-308. https://doi.org/10.1007/s13346-012-0124-9
27. Lee, H., Hwang, D., Lee, M., Lee, J., Cho, S., Kim, T. J., & Kim, H. S. (2022). Micro-Current Stimulation Suppresses Inflammatory Responses in Peptidoglycan-Treated Raw 264.7 Macrophages and Propionibacterium acnes-Induced Skin Inflammation via TLR2/NF-κB Signaling Pathway. *Int J Mol Sci*, *23*(5). https://doi.org/10.3390/ijms23052508
28. Li, C., Zheng, X., Hu, M., Jia, M., Jin, R., & Nie, Y. (2022). Recent progress in therapeutic strategies and biomimetic nanomedicines for rheumatoid arthritis treatment. *Expert Opin Drug Deliv*, *19*(8), 883-898. https://doi.org/10.1080/17425247.2022.2094364
29. Li, H., Xu, D., Cai, W., Liu, J., Bing, Z., & Zhang, Q. (2025). PEGylated Nanoliposomal Doxorubicin Conjugated with Specific TREM2 Peptides for Glioma-Targeting Therapy. *Adv Healthc Mater*, *14*(4), e2403096. https://doi.org/10.1002/adhm.202403096
30. Li, N., Du, Q., Jing, Z., Xue, L., He, W., Zhang, X., & Sun, Z. (2022). Study of the effects of Au@ZIF-8 on metabolism in mouse RAW 264.7 macrophages. *Biomater Adv*, *138*, 212800. https://doi.org/10.1016/j.bioadv.2022.212800
31. Li, Y., Zhang, H., Wei, J., Jin, W., Tong, Q., Ye, Y., Xie, Q., Li, Q., Cheng, G., & Xiong, Y. (2025). Celastrol liposomes enhance anti-PD-L1 in triple-negative breast cancer by reprogramming immunosuppressive microenvironment driven by cancer-associated adipocytes. *Phytomedicine*, *148*, 157275. https://doi.org/10.1016/j.phymed.2025.157275
32. Liang, Z., Xu, J. P., Meng, X. L., Lu, W., Wang, J., & Xia, H. (2009). Improve bioavailability of Harpin protein on plant use PLGA based nanoparticle. *J Biotechnol*, *143*(4), 296-301. https://doi.org/10.1016/j.jbiotec.2009.08.004
33. Lin, S., Zhou, Z., Xu, C., Zeng, F., Shi, Z., Sun, J., Mei, X., Liu, C., & Li, D. (2022). Cytokine Regulation and Fast Inflammation Resolution in Early Rheumatoid Arthritis by Cerium-Modified Gold Nanoclusters. *ACS Appl Mater Interfaces*, *14*(16), 18053-18063. https://doi.org/10.1021/acsami.1c22831
34. Liu, Y., Song, J., Guo, Y., Li, S., Yuan, M., Tang, J., Wang, Y., Li, M., Guo, Y., & Guo, L. (2025). Synergistic therapy with celastrol-curcumin multifunctional nanomedicine: Anti-hepatocellular carcinoma and reduced hepatotoxicity. *Int J Pharm*, *671*, 125289. https://doi.org/10.1016/j.ijpharm.2025.125289
35. Lü, J. M., Wang, X., Marin-Muller, C., Wang, H., Lin, P. H., Yao, Q., & Chen, C. (2009). Current advances in research and clinical applications of PLGA-based nanotechnology. *Expert Rev Mol Diagn*, *9*(4), 325-341. https://doi.org/10.1586/erm.09.15
36. Mias, C., Chansard, N., Maitre, M., Galliano, M. F., Garidou, L., Mengeaud, V., Bessou-Touya, S., & Duplan, H. (2023). Myrtus communis and Celastrol enriched plant cell culture extracts control together the pivotal role of Cutibacterium acnes and inflammatory pathways in acne. *J Eur Acad Dermatol Venereol*, *37 Suppl 2*, 12-19. https://doi.org/10.1111/jdv.18793
37. Mino, M., Yamasaki, M., Nabeshima, S., Fujimoto, Y., Kurushima, H., Taniwaki, M., Matsumoto, N., Kawamoto, K., Izumi, Y., Otohara, M., & Hattori, N. (2021). Cryptococcal Meningitis in a Patient With Rheumatoid Arthritis Treated With Abatacept. *J Clin Rheumatol*, *27*(8s), S701-s702. https://doi.org/10.1097/rhu.0000000000001597
38. Mohamed, S. A., Eraqi, W. A., Georghiou, P. E., & Zakaria, M. Y. (2025). Luteolin loaded PEGylated cerosomes: a novel treatment for MRSA skin infections. *BMC Microbiol*, *25*(1), 182. https://doi.org/10.1186/s12866-025-03873-0
39. Mori, S., Ogata, F., & Tsunoda, R. (2021). Risk of venous thromboembolism associated with Janus kinase inhibitors for rheumatoid arthritis: case presentation and literature review. *Clin Rheumatol*, *40*(11), 4457-4471. https://doi.org/10.1007/s10067-021-05911-4
40. Ostróżka-Cieślik, A. (2025). Hyaluronan-Based Hydrogel Hybrid Insulin Carriers-Preformulation Studies. *Polymers (Basel)*, *17*(19). https://doi.org/10.3390/polym17192661
41. Ozdemir, O., Agras, P. I., Hizli, S., Guveloglu, M., & Kabakus, N. (2009). Eisenmenger syndrome and juvenile rheumatoid arthritis--a case of double diagnosis. *Kardiol Pol*, *67*(12), 1377-1380.
42. Qi, M., Zhang, K., Zhang, X., Zhu, Y., Cai, B., Wang, C., Zhao, G., Zhang, D., & Zhang, J. (2025). Arginine tagged liposomal carrier for the delivery of celastrol for ferroptosis-induced hepatocellular carcinoma therapy. *Colloids Surf B Biointerfaces*, *250*, 114546 https://doi.org/10.1016/j.colsurfb.2025.114546

43. Qiu, F., Xi, L., Chen, S., Zhao, Y., Wang, Z., & Zheng, Y. (2021). Celastrol Niosome Hydrogel Has Anti-Inflammatory Effect on Skin Keratinocytes and Circulation without Systemic Drug Exposure in Psoriasis Mice. *Int J Nanomedicine*, *16*, 6171-6182. https://doi.org/10.2147/ijn.S323208
44. Quan, P., Jiao, B., Shang, R., Liu, C., & Fang, L. (2021). Alternative therapy of rheumatoid arthritis with a novel transdermal patch containing Siegesbeckiae Herba extract. *J Ethnopharmacol*, *265*, 113294 https://doi.org/10.1016/j.jep.2020.113294
45. Rahali, K., Tabriz, A. G., & Douroumis, D. (2025). Quality by design (QbD) liposomes engineering using 3D printed Tesla microfluidic arrays. *J Liposome Res*, *35*(4), 357-369. https://doi.org/10.1080/08982104.2025.2504018
46. Rajkumari, A., Kataki, M. S., Pal, P., Singh, M., Jana, B. K., & Mazumder, B. (2024). Development and Characterization of Lycopene Encapsulated Surface-Engineered Pegylated PLGA Nanoparticles for Enhanced Bioavailability and Active Targeted Delivery in Breast Cancer Using MNU-Induced Tumor Model.
47. Rathore, P., Gupta, R., Singh, P. P., Awasthi, A., Kishore, A., Bansal, K. K., & Mahor, A. K. (2025). QbD-Based Development of Fluocinolone Nanocomposite Transdermal Gel: Optimization, Characterization, and Enhanced Anti-hyperpigmentation Efficacy Assessment. *AAPS PharmSciTech*, *26*(4), 100. https://doi.org/10.1208/s12249-025-03094-8
48. Santos, C. I. M., Cicuéndez, M., Gonçalves, G., Rodríguez-Pérez, L., Portolés, M. T., Faustino, M. A. F., Herranz, M., Neves, M., Martinho, J. M. G., Maçôas, E. M. S., & Martín, N. (2023). Safety assessment of new nanodiamonds@corrole hybrids addressed by the response of RAW-264.7 macrophages. *J Mater Chem B*, *11*(3), 675-686. https://doi.org/10.1039/d2tb01863b
49. Sathishbabu, P., Uthaiah, C. A., & Hani, U. (2025). Comprehensive evaluation of EGFR and AKT targeting efficacy of resveratrol loaded PEGylated liposomes for the glioblastoma management: In silico, in vitro BBB permeation studies. *Bioorg Chem*, *154*, 108077. https://doi.org/10.1016/j.bioorg.2024.108077
50. Schattner, A. (2023). The Cardiovascular Burden of Rheumatoid Arthritis - Implications for Treatment. *Am J Med*, *136*(12), 1143-1146. https://doi.org/10.1016/j.amjmed.2023.09.004
51. Shao, Y., Zhang, H., Shi, Q., Wang, Y., & Liang, Q. (2023). Clinical prediction models of rheumatoid arthritis and its complications: focus on cardiovascular disease and interstitial lung disease. *Arthritis Res Ther*, *25*(1), 159. https://doi.org/10.1186/s13075-023-03140-5
52. Singh, R., Jadhav, K., Vaghasiya, K., Ray, E., Shukla, R., & Verma, R. K. (2023). New Generation Smart Drug Delivery Systems for Rheumatoid Arthritis. *Curr Pharm Des*, *29*(13), 984-1001. https://doi.org/10.2174/1381612829666230406102935
53. Sintayehu, B., Kakoti, B. B., Kataki, M. S., Gebrelibanos, M., Periyasamy, G., Aynalem, A., Zeru, H., & Asres, K. (2017). Hepatoprotective, Antioxidant and Anticancer Activities of Terminalia brownii Fresen Leaf Extract. *Ethiop. pharm. J*, *33*, 29-38.
54. Srivastava S, Kamthania M, Singh S, Saxena AK, Sharma N. Structural basis of development of multi-epitope vaccine against Middle East respiratory syndrome using in silico approach. Infect Drug Resist. 2018 Nov 21;11:2377-2391. doi: 10.2147/IDR.S175114. PMID: 30538505; PMCID: PMC6254671.
55. Steele, G., & Austin, T. (2016). Preformulation investigations using small amounts of compound as an aid to candidate drug selection and early development. In *Pharmaceutical Preformulation and Formulation* (pp. 29-140). CRC Press.
56. Tan, J. L., Yi, J., Cao, X. Y., Wang, F. Y., Xie, S. L., Zhou, L. L., Qin, L., & Dai, A. G. (2023). Celastrol: The new dawn in the treatment of vascular remodeling diseases. *Biomed Pharmacother*, *158*, 114177. https://doi.org/10.1016/j.biopha.2022.114177
57. Thakur, C. K., Thotakura, N., Kumar, R., Kumar, P., Singh, B., Chitkara, D., & Raza, K. (2016). Chitosan-modified PLGA polymeric nanocarriers with better delivery potential for tamoxifen. *International journal of biological macromolecules*, *93*(Pt A), 381-389. https://doi.org/10.1016/j.ijbiomac.2016.08.080
58. *Umesh Kumar, Manisha S. Nangude, Indu Mittal, Dommaraju R. Aruna Kumari, Kavuru Srivalli and Ridhi Bajaj* .Development and biological evaluation of piperine-loaded chitosan nanoparticles for enhanced anti-inflammatory and cytotoxic activity against colorectal cancer cells. Journal of Experimental Zoology,India 2026, Volume: 29, Issue No: 1(January), Page No: 947. **DOI: 10.51470/jez.2026.29.1.947**
59. Xian, J., Zhong, X., Gu, H., Wang, X., Li, J., Li, J., Wu, Y., Zhang, C., & Zhang, J. (2021). Colonic Delivery of Celastrol-Loaded Layer-by-Layer Liposomes with Pectin/Trimethylated Chitosan Coating to Enhance Its Anti-Ulcerative Colitis Effects. *Pharmaceutics*, *13*(12). https://doi.org/10.3390/pharmaceutics13122005
60. Yang, H., Tyagi, P., Kadam, R. S., Holden, C. A., & Kompella, U. B. (2012). Hybrid dendrimer hydrogel/PLGA nanoparticle platform sustains drug delivery for one week and antiglaucoma effects for four days following one-time topical administration. *ACS Nano*, *6*(9), 7595-7606, Article 22876910. https://pubmed.ncbi.nlm.nih.gov/22876910/
61. Zhang, Y., Liu, R., Li, C., Shi, L., Guo, Z., Zhu, L., Li, W., Li, J., & Li, Z. (2022). Celastrol-based nanomedicine hydrogels eliminate posterior capsule opacification. *Nanomedicine (Lond)*, *17*(20), 1449-1461. https://doi.org/10.2217/nnm-2022-0191